Nuclear Magnetic Resonance Studies of Carbon Dioxide Capture

Suzi M. Pugh, Alexander C. Forse*

Yusuf Hamied Department of Chemistry, Lensfield Road, Cambridge, CB21EW, U.K.

*corresponding author: acf50@cam.ac.uk

Abstract

Carbon dioxide capture is an important greenhouse gas mitigation technology that can help limit climate change. The design of improved capture materials requires a detailed understanding of the mechanisms by which carbon dioxide is bound. Nuclear magnetic resonance (NMR) spectroscopy methods have emerged as a powerful probe of CO_2 sorption and diffusion in carbon capture materials. In this article, we first review the practical considerations for carrying out NMR measurements on capture materials dosed with CO_2 and we then present three case studies that review our recent work on NMR studies of CO_2 binding in metal-organic framework materials. We show that simple ^{13}C NMR experiments are often inadequate to determine CO_2 binding modes, but that more advanced experiments such as multidimensional NMR experiments and ^{17}O NMR experiments can lead to more conclusive structural assignments. We further discuss how pulsed field gradient (PFG) NMR can be used to explore diffusion of adsorbed CO_2 through the porous framework. Finally, we provide an outlook on the challenges and opportunities for the further development of NMR methodologies that can improve our understanding of carbon capture.

Introduction to Carbon Dioxide Capture

The climate change crisis requires large-scale human behaviour changes and the rapid deployment of a range of greenhouse gas emissions mitigation technologies. Among these, carbon dioxide capture and storage is an important technology that can reduce emissions from point sources.[1] In this approach, CO_2 is captured from gas emissions at industrial sources that may include power stations, hydrogen production plants, cement factories and steel factories. This is achieved using a capture material that selectively absorbs CO_2 from the mixture of emitted gases (**Figure 1**). The CO_2 is then collected from the capture material *via* the application of heat (and/or a vacuum) and is subsequently stored in the ground where it can be permanently sequestered. A closely related technology is direct air capture, where a capture material is instead used to capture and remove carbon dioxide directly from the atmosphere. If the carbon dioxide is then collected and stored securely, this technology can offer "negative emissions", which are increasingly thought to be important in climate change mitigation pathways.[2]
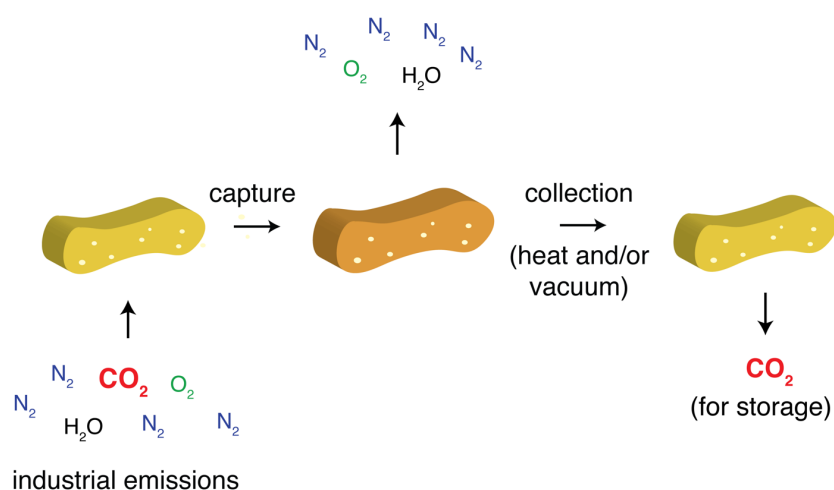

Figure 1. Schematic of CO_2 capture from industrial emissions. A capture material selectively binds CO_2, collecting it from the gas mixture. To collect the CO_2 for storage and regenerate the capture material, energy is normally supplied in the form of heat or a reduced pressure.

A good carbon capture material for must generally have (i) large CO_2 capture capacities, (ii) highly selective CO_2 uptake, (iii) fast uptake kinetics, (iv) low energy consumption (joules per kg CO_2 captured), and (v) long term stability to repeated cycling. The most established technology for point source carbon capture employs aqueous amine solutions to capture CO_2 and is used in a number of large-scale demonstration projects. However, this technology has some limitations including relatively large energy consumption for regeneration, corrosion of the steel containers in which the amines are housed, and amine degradation (*e.g.* by oxidation).[3] An active area of research is, therefore, to design new capture materials with improved performance.[4–9]

A large range of new carbon capture materials are under consideration, not limited to advanced amine solvents, ionic liquids and solid sorbents.[4–9] In this article we focus on solid sorbents, which are generally porous materials that bind CO_2 at their internal surfaces (inside their pores). A wide range of porous materials including metal-organic frameworks (MOFs), porous silicas, activated carbons and porous polymers have been explored for CO_2 capture. For example, a MOF was recently reported to have excellent performance for CO_2 capture via the physical adsorption of CO_2 in the pores of the material.[10] Another promising strategy is to functionalise porous materials with reactive functional groups such as amines or hydroxides. For example, amine-functionalised MOFs have shown promising performance and have enabled new adsorption mechanisms with unusual adsorption thermodynamics (see below).[11,12]

The design of improved carbon dioxide capture materials requires a detailed understanding of how carbon dioxide binds and moves within capture materials. Characterisation of carbon capture chemistry is often challenging and requires the use of a wide range of experimental techniques as well as simulation methods. Among these methods, nuclear magnetic resonance (NMR) spectroscopy has emerged as a powerful probe of binding chemistry and molecular dynamics. NMR experiments can be performed on liquids, solids and gases, as well as samples containing a variety of phases. In the case of solid materials, there is no requirement for crystallinity and amorphous materials can readily be studied. In this article, we review the practical considerations for carrying out NMR studies of carbon dioxide capture. We then show three case studies of how NMR methods have been developed to understand CO_2 adsorption and diffusion mechanisms in MOFs.[13–15]

**Practical Considerations for NMR Studies of Carbon Dioxide Capture**

The first practical consideration is which nucleus to study. Many studies directly probe the bound CO_2 molecules by ^{13}C NMR spectroscopy. As a spin 1/2 nucleus ^{13}C can readily be studied with a wide range of NMR techniques, though the low natural abundance of ^{13}C (1.11 %) may require the use of signal enhancement techniques, especially since T_1 relaxation times are often long for ^{13}C. The use of ^{13}C-enriched CO_2 is generally very helpful for increasing the signal to noise ratios and enabling more advanced experiments. Beyond ^{13}C NMR, ^{17}O NMR may be used to directly study the CO_2 molecules.[14,16] The very low natural abundance of this isotope (0.037 %) generally means that enrichment is likely to be essential for most experiments. Since ^{17}O is a spin 5/2 quadrupolar nucleus, solid-state experiments require the use of high magnetic fields and multi-dimensional experiments to resolve closely related chemical environments (see later).[14] Beyond directly studying the captured CO_2, insight into the capture behaviour can be gained by studying additional NMR-active nuclei present in the capture material. For example, ^{15}N NMR experiments have been used in amine-based materials, where reaction generally occurs at the nucleophilic nitrogen centres.[13,17–20]

A critical further consideration for NMR spectroscopy studies of carbon dioxide capture is how to prepare and study the sample in the presence of CO_2. NMR experiments of carbon dioxide capture may be categorized according to whether they are performed with sample magic angle spinning (MAS), or with static sample conditions (**Figure 2**). Experiments may then be further categorised into *ex situ* and *in situ* experiments, where *ex situ* refers to experiments on samples that are dosed with CO_2 and sealed in the laboratory prior to NMR studies, while *in situ* refers to dosing the sample with gas inside the magnet while simultaneously studying it with NMR methods (**Figure 2**). Each of these approaches has advantages and disadvantages, and the optimum method will depend on the exact materials studies and the desired information. Importantly, safety must always be the top priority. CO_2 is a colourless and odourless gas at ambient conditions. Exposure to CO_2 may cause headaches, dizziness, confusion and loss of consciousness. At high levels of exposure, death by asphyxiation could occur (note that CO_2 is heavier than air, and can accumulate in the laboratory in some scenarios).
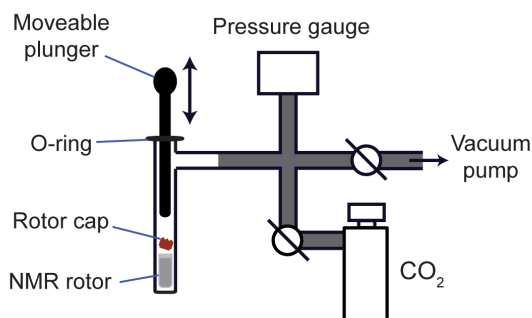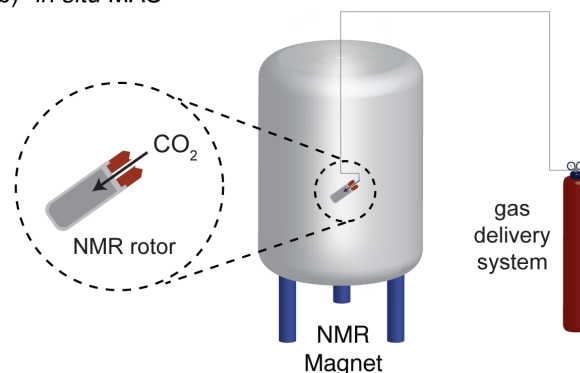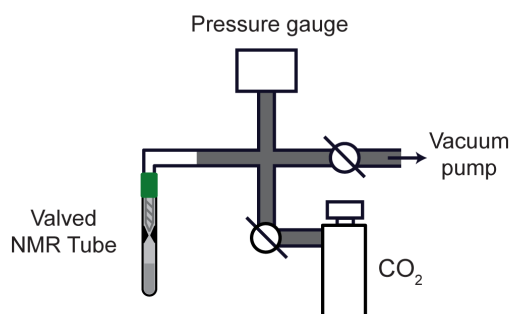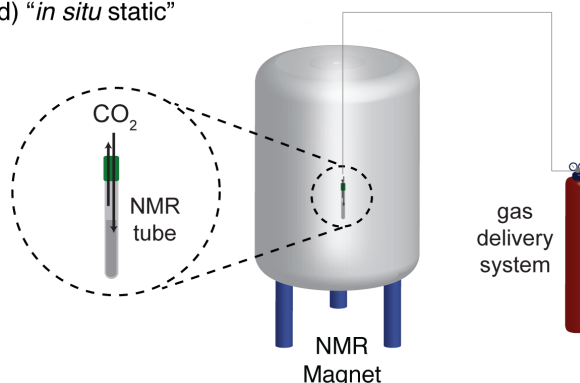

Figure 2. Approaches for studying CO_2 capture materials with NMR spectroscopy. a) and b) use MAS conditions for the NMR measurement, which c) and d) perform measurements under static conditions. In a) and c) the sample is loaded with CO_2 *ex situ*, and then taken to the magnet for NMR studies. In b) and d), the CO_2 is dosed inside the magnet, referred to as *in situ*.

Figure 2a shows a common *ex situ* approach for studying solid-adsorbents for CO_2 capture, which we term "*ex situ* MAS".[13,17,21] In this approach, a MAS rotor is packed with the solid adsorbent and is transferred to a gas-dosing manifold, with the rotor left open. The sample is then evacuated before dosing CO_2 gas. Following a period of equilibration, the sample is sealed, for example by using a mechanical plunger, and is then removed for MAS magnetic resonance experiments.[13] An advantage of this approach is that standard MAS rotors and probes are used, which can greatly improve spectral resolution for solid samples. If the gas-dosing manifold is designed to have a low volume, isotopically enriched gases can also be readily used (*e.g.* $^{13}CO_2$) to improve signal intensities. A clear disadvantage of this approach is that it is time-consuming to study multiple gas-dosing conditions (*e.g.* different gas-dosing pressures, different gas-dosing temperatures). A further disadvantage is that the dosed gas may escape from the MAS rotor over time (depending on how strong the adsorption is, and how leak-tight the rotor is). In cases where bespoke rotor dosing equipment is not available, simple alternatives such as a gas-filled glovebag or chamber may also be employed, provided appropriate safety measures are taken to avoid CO_2 exposure. The *ex situ* MAS approach has been applied to a range of solid-adsorbent materials to study carbon capture modes. A number of studies have explored carbon capture chemistry in amine-functionalised silicas,[20–26] metal-organic frameworks,[8,27–32] amine-functionalised metal-organic frameworks,[11,13,14,33–36] zeolites,[37–40] polymers,[41] and porous carbons.[42]

The disadvantages of the *ex situ* MAS approach can be partly resolved by the "*in situ* MAS" approach (**Figure 2b**). Here MAS NMR experiments are performed on the solid adsorbent sample with the simultaneous delivery of CO_2 gas to the sample via a hole in one of the rotor caps.[43–45] This approach has the advantages that the sample is studied directly under operating conditions, and that the gas dosing conditions (sample temperature and partial pressure of CO_2) can be varied continuously. Kinetic studies should also be accessible with this approach.[43] One potential disadvantage is the potentially high cost of flowing isotopically enriched gases unless a gas recovery system can be employed. The flow of gases also requires more careful planning with regard to safety issues surrounding gas exposure. When setting up *in situ* experiments, a further safety consideration is that one must avoid bringing any magnetic parts close to the magnet (e.g. for the gas delivery system). Initial experiments with the *in situ* MAS approach on amine-functionalised silicas highlight the great promise of this approach.[43]

Two further approaches may be considered that employ NMR measurements on static samples. These can be applied to both liquid absorbents and solid adsorbents. In the "*ex situ* static" approach, CO_2 is introduced to the sample in an NMR tube, either by bubbling CO_2 through a liquid or by dosing CO_2 into a solid with a gas manifold (**Figure 2c**).[13–15,46] After the sample has equilibrated, the tube is

sealed and taken for NMR experiments. A key advantage of this approach is that only conventional solution-state NMR spectroscopy equipment is required and that both liquid absorbents and solid adsorbents can be studied. A clear disadvantage is that MAS experiments are not possible. However, we do note that MAS is not required for liquid absorbents (where molecular motion averages out anisotropic interactions), nor for many solid adsorbents, where the considerable motion of CO_2 (especially for physisorbed CO_2, with only non-covalent CO_2-adsorbent interactions) can lead to relatively narrow peaks for adsorbed CO_2. This method has been used to study a wide range of materials including ionic liquids[7,47,48] and metal-organic frameworks.[8,15]

Finally, the "*in situ* static" approach extends the above approach to directly dose CO_2 gas into the static sample during the acquisition of NMR data (**Figure 2d**).[49,50] This again has the advantage of enabling the capture material to be studied during operation, while also enabling a range of gas pressures and sample temperatures to be studied efficiently. One excellent example of these measurements explored the CO_2 absorption pathways in a wide range of state-of-the-art aqueous amine CO_2 absorbents.[50] CO_2 gas was bubbled through the aqueous amine solutions inside the NMR magnet, and NMR measurements were recorded as a function of time. These experiments revealed the time-dependent uptake mechanisms, which varied significantly depending on the exact choice of amine. For example, monoethanolamine initially captures CO_2 via the formation of ammonium carbamate, but at longer reaction times ammonium bicarbonate products began to dominate at the expense of the ammonium carbamates. A further excellent example used the "*in situ* static" approach to study mixed gas adsorption in a solid MOF adsorbent.[49] The role of framework flexibility on the selectivity of gas adsorption was explored.

Having reviewed the main practical details associated with NMR studies of carbon capture materials, we now give three case studies from our research on metal-organic frameworks to highlight the types of information that can be obtained.

Background on Metal-Organic Frameworks

MOFs are a class of microporous materials typically constructed from metal nodes and organic linkers to give three-dimensional framework structures. Their use as CO_2 sorbents is highly favourable owing to their high surface areas and the possibility to precisely control the pore chemistry. One emerging class of MOFs that have shown promise for CO_2 capture are amine-appended frameworks based on
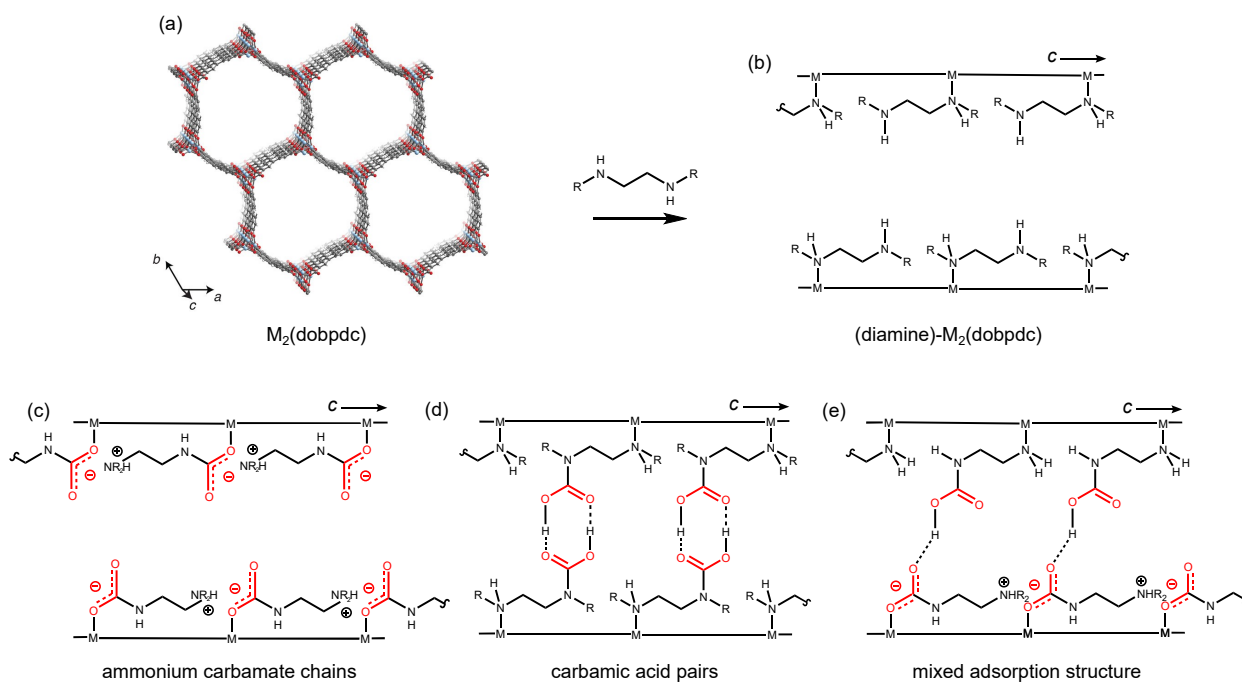
Figure 3. a) Structure of the M_2(dobpdc). Schematic representations of b) amine functionalisation yielding (amine)-M_2(dobpdc) and c-e) CO_2 adsorption products c) ammonium carbamate chains, d) carbamic acid pairs and e) mixed ammonium carbamate – carbamic acid.

the MOF-74 structure, such as M_2(dobpdc) where M = Mg, Mn, Fe, Co, Ni, Cu, Zn, Cd, and dobpdc = 4,4′-dioxidobiphenyl-3,3′-dicarboxylate (**Figure 3a**).[51] In this structure, the metal ion has a vacant coordination site along the microporous channels. The appendage of an organic amine compound to these vacant metal sites (**Figure 3b**) gives rise to large adsorption capacities for selective and reversible CO_2 uptake.[51] As the nature of both the metal cation and the amine can be varied, the adsorption thermodynamics can be tuned for a desired application.[12,33,35,42,46,52] Amine-appended MOF-74 analogues may be advantageous over other sorbent materials, as they display step-shaped adsorption isotherms, suggesting that CO_2 uptake/release is sudden upon exposure at a threshold pressure. As such, these materials have lower regeneration energies than traditional amine scrubbing technologies.[12]

Basic characterisation methods such as powder X-ray diffraction and solution state ^{1}H NMR of digested frameworks can be used in order to ascertain the long-range ordering of the material and to assess the amine loading, respectively. In these materials a 1:1 metal:amine ratio can be achieved, indicating that all initially vacant metal sites are occupied by amines (**Figure 3b**). X-ray crystallography studies on large single crystals of amine-appended-Zn_2(dobpdc) materials have shown that at least two types of CO_2 adsorption products can be formed in these materials. The first product is ammonium carbamate chains, where CO_2 inserts itself into the Metal-N bond to form a negatively charged carbamate (**Figure 3c**) and a neighbouring diamine forms a positive ammonium.

Adjacent carbamates and ammoniums form ion pairing and hydrogen bonding interactions to produce chains, explain the cooperative adsorption in these materials, and accounting for the step-shaped adsorption isotherms. The ammonium carbamate chain product has been observed for many diamine-Zn_2(dobpdc) analogues, and is thought to be the most prevalent product.[35] In (dmpn)$_2$-Zn_2(dobpdc) (dmpn = 2,2-dimethyl-1,3-diaminopropane), however, the formation of carbamic acid pairs was reported, whereby the CO_2 molecule reacts with a "dangling" primary amine, and two carbamic acids interact via hydrogen bonding to form a pair (**Figure 3d**).[33]

Unfortunately, structure solution by X-ray crystallography generally requires large single crystals which are difficult to synthesise for many analogues of M_2(dobpdc). The case studies presented here use multinuclear NMR spectroscopy to explore CO_2 adsorption on the molecular level without the need for large single crystals and can, therefore, be applied to many different amine analogues in these MOFs. Indeed, we will show how solid-state NMR studies on (dmpn)$_2$-Mg_2(dobpdc) materials revealed that CO_2 can adsorb by a third mechanism where both ammonium carbonate chains and carbamic acids are formed on adjacent metal sites, stabilised by hydrogen bonding (**Figure 3e**).[13]

Case Study 1: Elucidating Chemisorption in MOFs with ^{13}C and ^{1}H experiments

As discussed previously, ^{13}C NMR experiments can be implemented easily and provide a wealth of information about the number and type of carbon environments present in sorbent materials. More detailed information about the binding mechanisms can be gained by exploring the local connectivity of the carbon atoms through correlation experiments. However, this approach is typically limited by the low natural abundance of ^{13}C and as such, the use of isotopically enriched $^{13}CO_2$ gas and/or more complex sensitivity-enhanced experiments. In solids, the cross polarisation (CP) experiment can be used to transfer magnetisation *via* dipolar couplings from a high abundance, high γ nucleus, such as ^{1}H, to a low abundance, low γ nucleus, such as ^{13}C, thus increasing the sensitivity and decreasing spectral acquisition time. The build-up of magnetisation on the low γ nuclei is governed by the distance between the coupled spins, as well as molecular dynamics. By using short transfer pulses, only spins in close proximity will be selectively enhanced in the NMR spectrum and therefore the CP experiment can be used as a spectral editing technique. Longer-range couplings can be explored by increasing the transfer time, however, this build-up can be impeded by the $T_{1\rho}$ relaxation of the high γ nuclei and as such, the absolute intensities of signals in these experiments should be treated with care. Furthermore, cross polarisation can be used to transfer magnetisation in two-dimensional HETCOR experiments, which allows for the observation of correlations between coupled spins. For these experiments, an *ex situ* CO_2 loading approach is favoured to gain high-resolution spectra of the final adsorption products under MAS conditions. Here we present a case study showing how one-

dimensional ^{13}C MAS and two-dimensional ^{1}H-^{13}C HETCOR experiments can be used to investigate binding mechanisms in MOF materials.
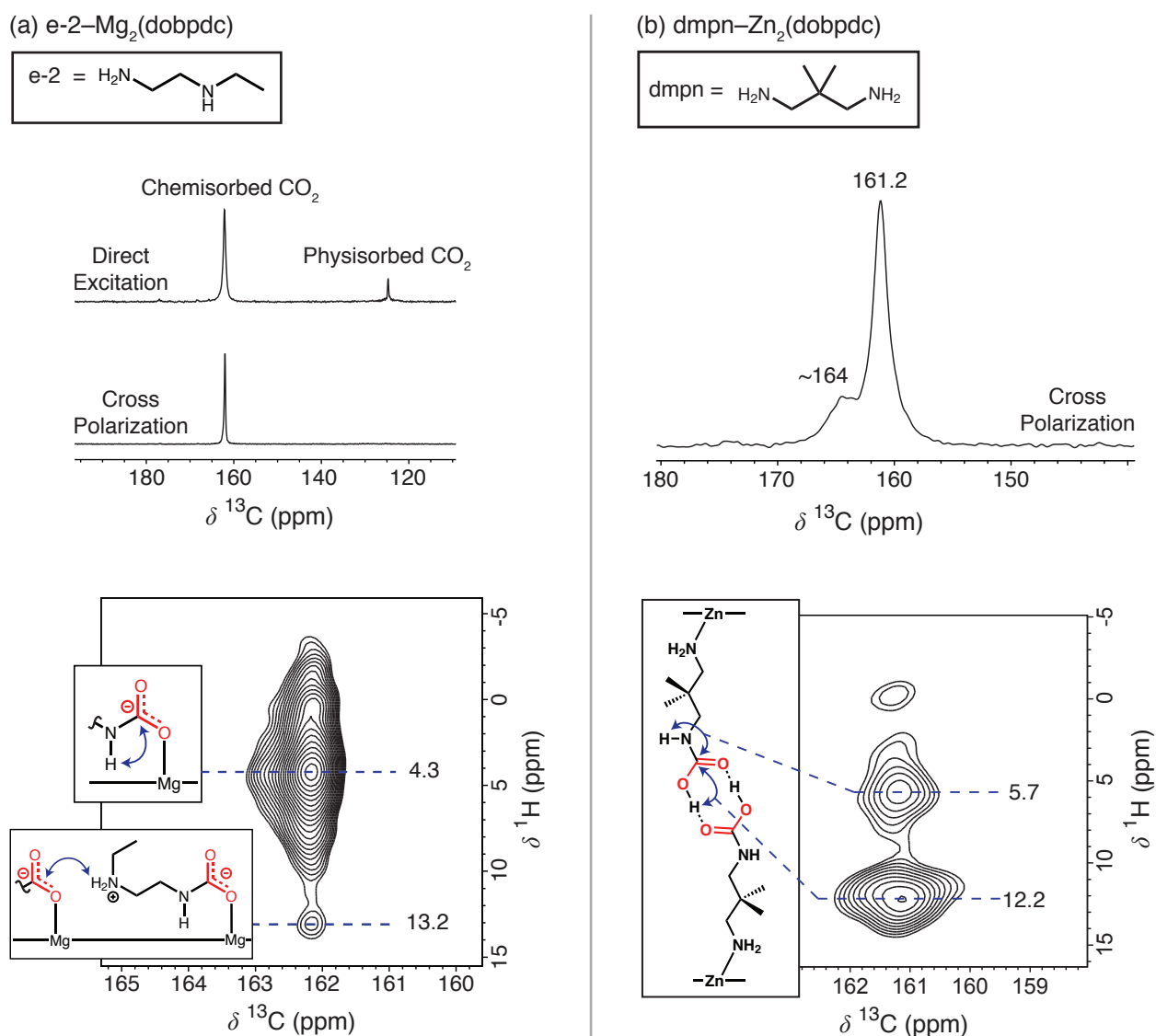

Figure 4. ^{13}C MAS (top) and ^{1}H-^{13}C HETCOR MAS (bottom) NMR (16.4 T) spectra for (e-2)Mg$_2$(dobpdc) and (dmpn)Mg$_2$(dobpdc) dosed at ~ 1 bar $^{13}CO_2$.

The ^{13}C NMR spectrum of (e-2)$_2$-Mg$_2$(dobpdc) (**Figure 4a,** e-2 = N-ethylethylenediamine) shows two peaks at 162.1 and 124.7 ppm, corresponding to chemisorbed and physisorbed CO_2, respectively.[13] The chemisorbed CO_2 signal is enhanced using a CP experiment and this signal is assigned to the formation of an ammonium carbamate chain upon CO_2 adsorption. In contrast, the (dmpn)$_2$-Zn$_2$(dobpdc) shows two chemisorbed CO_2 peaks with an intense signal at 161.2 ppm, assigned to carbamic acid pairs and a weaker signal at δ = 164 ppm, assigned to a small quantity of ammonium carbamates (**Figure 4b**). It is clear that the number and type of environments in (e-2)$_2$-Mg$_2$(dobpdc) and (dmpn)$_2$-Zn$_2$(dobpdc) are different, a range of ^{13}C chemical shift values are reported in the literature for ammonium carbamate chains and carbamic acids. The small differentiation in

chemical shifts between the similar ^{13}C environments in these mechanisms, therefore, means that the confidence in the assignments of these binding modes by ^{13}C MAS NMR spectroscopy alone is low.

To improve confidence in the peak assignments two-dimensional ^1H-^{13}C HETCOR experiments at short contact times were performed, allowing for the investigation of ^1H nuclei located near the $^{13}CO_2$ adsorption product.[13] The ^1H-^{13}C HETCOR experiment for (e-2)$_2$-Mg$_2$(dobpdc) (**Figure 4a**) shows a strong correlation of the chemisorbed CO_2 to a ^1H environment at δ = 4.3 ppm. This ^1H signal can be assigned to **H**NCOO$^-$, confirming the reaction of the CO_2 to the e-2 primary amine species. A weaker correlation can also be seen with a ^1H signal at δ = 13.2 ppm, arising from hydrogen bonding between the adsorption product and the secondary ammonium on an adjacent metal site. As such, these correlations provide greater evidence for ammonium carbamate chain formation. Conversely, in the ^1H-^{13}C HETCOR experiment for (dmpn)$_2$-Zn$_2$(dobpdc) (**Figure 4b**) two strong correlations are observed for the ^{13}C signal at δ = 161.2 ppm to ^1H signals at δ = 5.7 and 12.2 ppm, assigned to N**H**COOH and NHCOO**H**, respectively. These δ values are in good agreement with DFT calculations for carbamic acid pairs and these correlations are notably different from those observed for ammonium carbamate chains, thus providing greater confidence in the assignment of this adsorption mechanism for the (dmpn)$_2$-Zn$_2$(dobpdc).
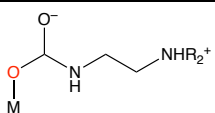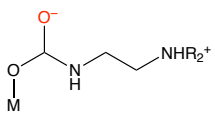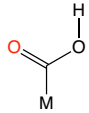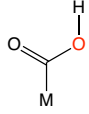
Case Study 2: ^{17}O NMR as a powerful new probe of CO_2 adsorption chemistry

Whilst ^1H and ^{13}C NMR spectroscopy can be useful probes of binding modes in amine-appended MOFs, the similar local environments surrounding the C atom makes unambiguous assignment of adsorption products difficult. There is a need to develop new techniques to unequivocally characterise these materials. From the adsorption mechanisms shown in **Figure 3**, it can be seen that each binding mode has two unique oxygen sites and the type of oxygen site present varies drastically depending on the binding mechanism. As such, ^{17}O NMR spectroscopy should be a highly diagnostic probe to study these materials. As discussed previously, the low natural abundance and quadrupolar nature of ^{17}O mean that isotopic enrichment and high magnetic field strengths are required to acquire NMR spectra. Furthermore, the quadrupolar interaction introduces a second-order broadening which cannot be removed by MAS. This coupling can be quantified by its magnitude (C_Q), defined as C_Q= eQV$_{zz}$/h, and the asymmetry (η_Q), defined as η_Q = V$_{xx}$–V$_{yy}$/V$_{zz}$, where e is the electronic charge, Q is the nuclear quadrupolar moment, h is Planck's constant and V$_{xx}$, V$_{yy}$ and V$_{zz}$ are the principle components of the electric field gradient tensor. The ^{17}O δ_{iso}, C_Q and η_Q can be determined by fitting the ^{17}O MAS spectrum. For spectra containing many overlapping ^{17}O signals, fitting the MAS spectrum can be challenging. This can be overcome by using two-dimensional MQMAS[53–55] or STMAS[56,57] experiments. The use of ^{17}O NMR spectroscopy, therefore, provides an additional set of parameters

compared to ^{13}C NMR spectroscopy, which can be used to classify CO_2 adsorption products. One drawback of this method is the relatively high cost of ^{17}O-enriched CO_2. This, therefore, precludes the use of *in situ* experiments where a flow system is used. Using an *ex situ* MAS method, acquisition of a high-resolution ^{17}O MAS NMR spectrum for amine-functionalised MOF materials can be achieved in approximately 30 minutes by dosing the sample at ~1 bar.[14] This translates to a cost of £50 per sample, although this value could be reduced by optimising the design (i.e., reducing the volume of gas in the system) of the experimental set up shown in **Figure 2a**.

To ascertain the value of ^{17}O NMR as a probe, the ^{17}O NMR parameters were calculated using DFT calculations for amine appended $Mg_2(dobpdc)$ containing a wide range of organic diamines.[14] The use of DFT calculations provides an excellent opportunity to explore and compare both known and novel adsorption products. Of the three adsorption mechanisms explored, ammonium carbamate chains, carbamic acid pairs and the mixed adsorption mechanism, four unique O environments were identified: M-**O**CO and M-OC**O**⁻, resulting from ammonium carbamate chains and C**O**OH and CO**O**H, resulting from the formation of carbamic acids. Each environment can be identified by their ^{17}O NMR parameters, as shown in **Table 1**. The key distinguishing feature for carbamic acids is the lower chemical shift, large C_Q and small η_Q values for the OH. Furthermore, in general, the metal bound oxygen can be distinguished from the carbamate O by a lower chemical shift. These calculations suggested that ^{17}O NMR spectroscopy is a powerful probe into these adsorption mechanisms. Experiments were then performed to explore this further.

Table 1. Summary of ^{17}O NMR parameters calculated for diamine-appended $Mg_2(dobpdc)$ structures.

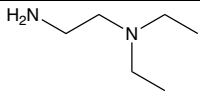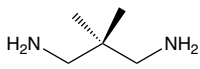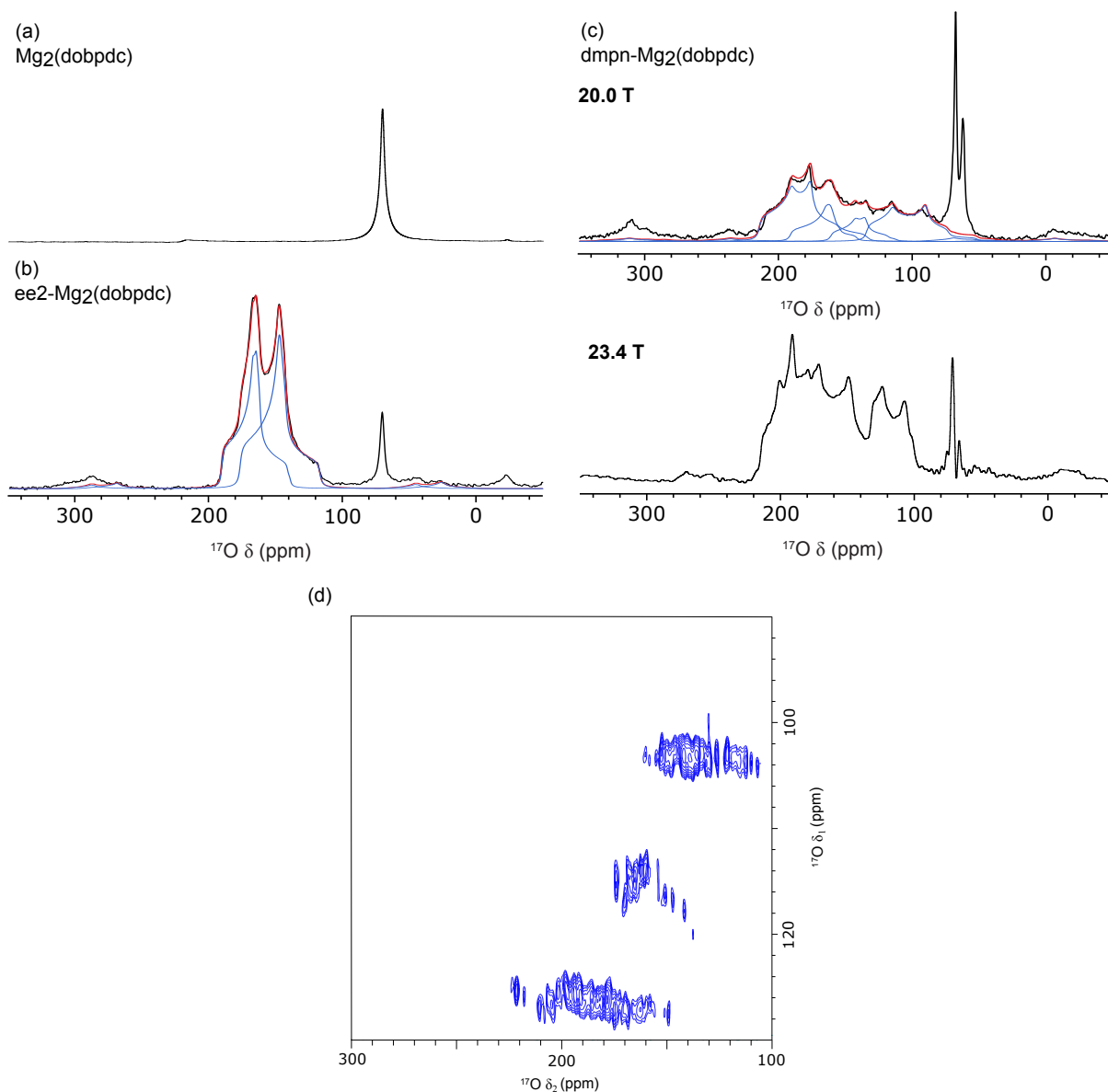|	Calculated ^{17}O NMR parameters		
	δ_{iso} (ppm)	C_Q /MHz	η_Q
	155 – 180	7.2 – 8.0	0.5 – 1
	150 – 230	6.5 – 7.8	0.5 – 1
	150 – 230	6.6 – 7.8	0.5 – 1
	110 – 150	8.0 – 8.4	0.3 – 0.5

Figure 5: (a-c) ^{17}O MAS NMR spectra of (a) bare Mg_2(dobpdc) (20.0 T, 12.5 kHz MAS) , (b) $C^{17}O_2$-ee2-Mg_2(dobpdc) (20.0 T, 12.5 kHz MAS) and (c) $C^{17}O_2$-dmpn-Mg_2(dobpdc) at 20.0 T (12.5 kHz MAS) (top) and 23.4 T (20 kHz MAS) (bottom) and (d) ^{17}O MQMAS NMR (20.0 T, 12.5 kHz MAS) of $C^{17}O_2$-dmpn-Mg_2(dobpdc).

Firstly, 'bare' Mg_2(dobpdc) (*i.e.*, where no amine has been appended to the vacant metal site) was dosed with $C^{17}O_2$. The resulting ^{17}O MAS NMR spectrum (**Figure 5a**) shows a single peak at δ = 61.5 ppm, corresponding to physisorbed CO_2 is present. This suggests that all chemisorption within these materials takes place as a result of interaction between the CO_2 and the amine.

The first amine-appended Mg_2(dobpdc) analogue chosen for study was (ee-2)$_2$-Mg_2(dobpdc); the binding mechanism in this material was confidently assigned as carbamate chain formation using the techniques discussed in Case Study 1. The ^{17}O MAS NMR spectrum, given in **Figure 5b**, shows three signals, corresponding to the two O environments in chemisorbed (δ = 100 - 200 ppm) and a signal at δ = 70.5 ppm corresponding to physisorbed CO_2. The extracted NMR parameters of these signals are consistent with the ^{17}O NMR parameters calculated using DFT (**Table 2**) for the formation of

ammonium carbamate chains and therefore the ^{17}O NMR spectroscopy confirms this binding mechanism for (ee-2)$_2$-Mg$_2$(dobpdc).

Table 2: Experimental and DFT-calculated ^{17}O NMR parameters for ee2-Mg$_2$(dobpdc) and dmpn Mg$_2$(dobpdc).

Compound	Amine Structure		^{17}O NMR parameters Experiment (DFT)		
			δ_{iso} (ppm)	C_Q /MHz	η_Q
(ee2)-Mg$_2$(dobpdc)		M-**O**CO	177 (169)	6.8 (7.4)	1.0 (1.0)
		M-OC**O**	91 (186)	6.4 (7.0)	0.8 (0.7)
(dmpn)-Mg$_2$(dobpdc)		M-**O**CO	168 (166)	6.9 (7.6)	0.8 (1.0)
		M-OC**O**	194 (183)	7.2 (7.2)	0.7 (0.9)
		C**O**OH	217 (230)	7.6 (7.9)	0.6 (0.5)
		CO**O**H	137 (131)	8.0 (8.2)	0.3 (0.4)

The second amine-appended Mg$_2$(dobpdc) material of interest is dmpn-Mg$_2$(dobpdc). As discussed previously, dmpn-Mg$_2$(dobpdc) is thought to capture CO$_2$ *via* a mixed adsorption mechanism, however, the assignment of this binding mechanism is not conclusive by ^1H and ^{13}C NMR spectroscopy owing to the overlap of signals for similar ^{13}C environments. Excitingly, the ^{17}O MAS spectrum (**Figure 5c**) for dmpn-Mg$_2$(dobpdc) showed a broad overlapping of multiple signals corresponding to chemisorption of CO$_2$ and two sharp resonances corresponding to physisorbed CO$_2$. To aid in the deconvolution of this spectrum, an ^{17}O MQMAS NMR spectrum was acquired (**Figure 5d**). This spectrum shows 3 signals and the extracted NMR parameters were consistent with the calculated δ_{iso}, C_Q and η_Q values for COO and M-COO, suggesting the formation of carbamate chains and a C=O in the mixed adsorption structure (Table 2). However, when fitting these signals to the ^{17}O MAS spectrum, an additional signal at lower chemical shifts is required to fully represent the whole spectral line shape. Deconvolution of the ^{17}O MAS spectrum with 4 signals shows that this additional peak can be assigned to carbamic acid OH resonance. This resonance is likely missing in the ^{17}O MQMAS NMR spectrum owing to inefficiencies in exciting MQ transitions for nuclei with large quadrupolar couplings and/or relaxation effects. To confirm these results, a ^{17}O MAS spectrum was recorded at 23.4 T (**Figure 5c**. The signal corresponding to COOH is now well-resolved from the other overlapping signals, allowing for increased confidence in the deconvolution of the spectrum acquired at 20.0 T. ^{17}O NMR spectroscopy has, therefore, provided conclusive evidence for the formation of the mixed adsorption structure and, excitingly, has provided the first unambiguous evidence of the formation of carbamic acid species in amine appended Mg$_2$(dobpdc) analogues

(**Table 2**). Overall, the work presented in case study 2 shows that ^{17}O NMR spectroscopy is a powerful probe to explore CO_2 binding mechanisms in metal-organic frameworks.

Case Study 3: Measuring anisotropic in-pore CO_2 diffusion in MOFs

CO_2 diffusion is an important physical phenomenon that influences the CO_2 capture performance of porous solid adsorbents. Following on from earlier studies that measured CO_2 diffusion in MOFs with pulsed-field gradient NMR (PFG NMR) methods,[58,59] we explored CO_2 diffusion in the material $Zn_2(dobdc)$ ($dobdc^{4-}$ = 2,5-dioxidobenzene-1,4-dicarboxylate). Similar to the $M_2(dobpdc)$ materials discussed above, this material features one-dimensional hexagonal channels in an ordered lattice (**Figure 6a**). The Zn(II) ions have a vacant coordination site, which is the primary binding site for CO_2. The one-dimensional pores of this material, and the lack of connectivity between different pores in the crystal structure, should result in a significant diffusion anisotropy, *i.e.* CO_2 self-diffusion along the pores ($D_{//}$) is anticipated to be much faster than diffusion between pores $D_{\perp}$.

First, large rod-like crystals of $Zn_2(dobdc)$ with lengths of 100s of microns were synthesised via a solvothermal method (**Figure 6a**).[60] In these crystals the hexagonal pores run along the length of the rods. The availability of such large crystals ultimately simplifies the PFG NMR analysis, since exchange of CO_2 between different crystals and with free CO_2 gas becomes negligible on the experimental timescales (typically tens of milliseconds for PFG NMR experiments). With large crystals in hand, the "*ex situ* static" approach was used whereby a large number of crystals were loaded into a valved NMR tube, which was dosed with $^{13}CO_2$, and then taken for static ^{13}C NMR measurements (**Figure 6b**).

A static ^{13}C NMR spectrum revealed a signal with a chemical shift consistent with physisorbed CO_2 as expected, and with a lineshape consistent with an anisotropic chemical shift observed for the adsorbed CO_2 (**Figure 6b**). While the lineshape is much narrower than that reported for solid CO_2,[61] the observed chemical shift anisotropy suggests that CO_2 molecules have a preferred average orientation relative to the framework pores, consistent with other studies of similar frameworks.[28,62] For the conditions studied in **Figure 6b**, signal intensity at the left hand edge of the spectrum with a chemical shift $\delta_{//}$ could be assigned to CO_2 adsorbed in crystals oriented parallel to the applied magnetic field, while signal intensity at the right hand edge could be assigned to CO_2 adsorbed in crystals oriented perpendicular to the applied magnetic field $\delta_{\perp}$.
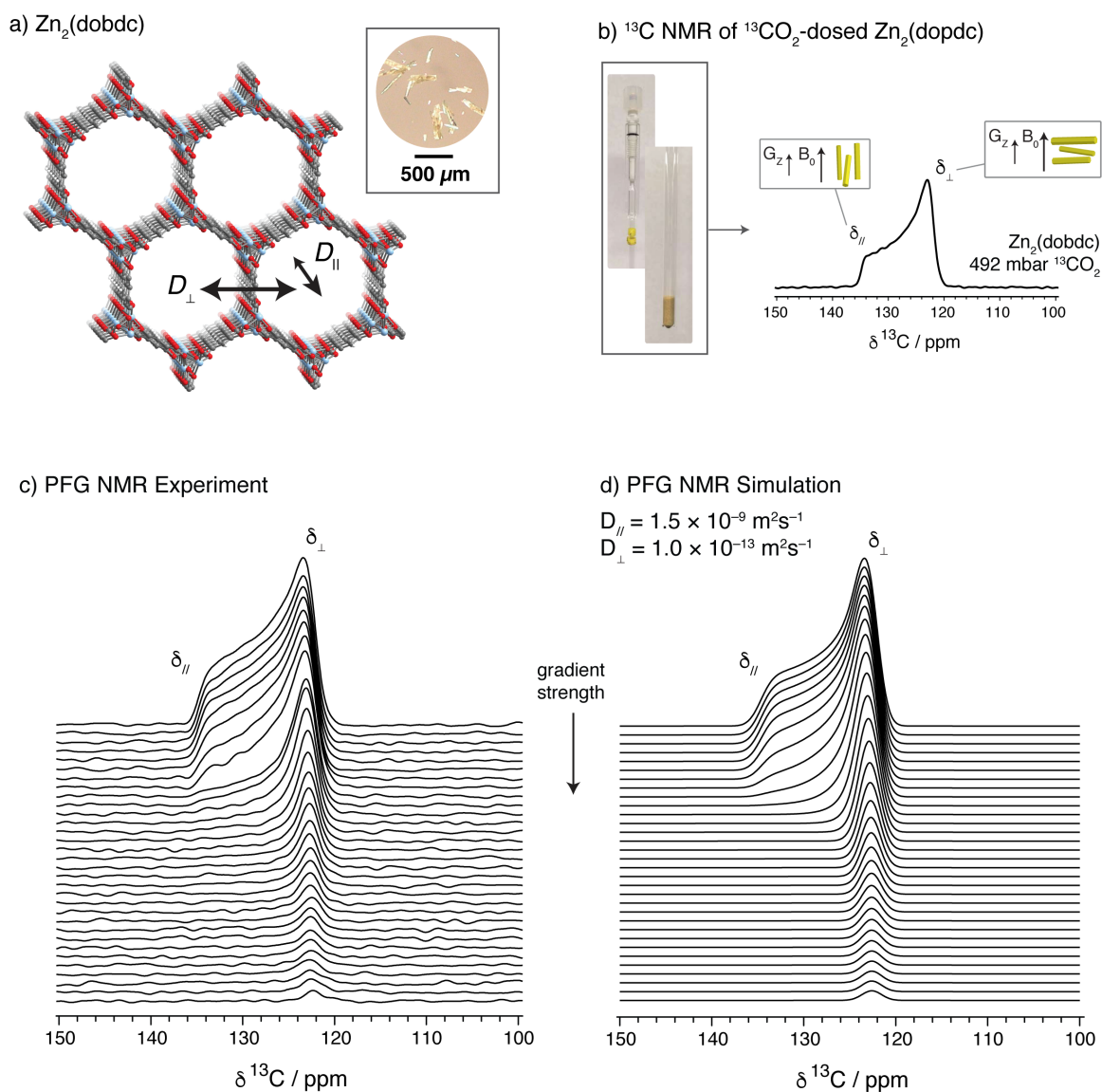
Figure 6. a) A portion of the crystal structure of the MOF $Zn_2(dobdc)$. Inset: microscope image showing the rod-like structure of the MOF crystals. b) static ^{13}C NMR spectrum of $Zn_2(dobdc)$ dosed with $^{13}CO_2$ gas. Inset: photograph of the valved NMR tube containing the gas-dosed crystals. c) Experimental and d) simulated PFG NMR spectra.

As was realised in earlier PFG NMR studies,[58,59,63] the observation of a chemical shift anisotropy lineshape provides an excellent opportunity for the measurement of anisotropic diffusion. Indeed, as the gradient strength was increased in a series of PFG NMR experiments, clear lineshape changes are observed (**Figure 6c**), which arise from the anisotropic diffusion of CO_2. In these experiments, the pulsed field gradient was applied along the laboratory z-axis, *i.e.* co-linear with the main applied magnetic field, B_0. Therefore, the rapid decay of signal intensity at the left hand edge of the spectrum corresponds to the relatively fast self-diffusion along the length of the rod-like crystals, *i.e.* along the hexagonal pores of the metal-organic framework. On the other hand, the much slower decay of signal intensity at the right hand edge of the spectrum reports on the much slower diffusion of CO_2 perpendicular to the MOF pores. Inspection of the spectra in **Figure 6c** therefore confirms the

anticipate result that $D_{//} \gg D_{\perp}$. The above arguments were also substantiated by additional experiments in which the magnetic field gradients were instead applied along the laboratory x-axis.

Inspired by earlier work,[58] spectral simulations were then performed to enable a more quantitative analysis (**Figure 6d**).[60,64] The only free parameters in the simulations are $D_{//}$ and $D_{\perp}$. The simulations shown in **Figure 6d** suggested that CO_2 diffusion along the framework pores takes a value of $D_{//} = D_{//} = 1.5(4) \times 10^{-9}$ m^{2}s^{-1}. This value is comparable to liquid water diffusion at ambient conditions, and is 4 orders of magnitude slower than the diffusion of free CO_2 gas. For diffusion of CO_2 between the MOF pores, we were only able to conclude an upper limit of $D_{\perp} < 10^{-13}$ m^{2}s^{-1}, and it was not possible to conclude whether or not $D_{\perp}$ had non-zero value. These findings show that the CO_2 diffusion between the MOF channels is at least 10,000 times slower than diffusion along the MOF channels, *i.e.* the diffusion is very strongly anisotropic. This finding has implications for the practical applications of these materials, and suggests that rod-like crystals are in-fact not desired for practical applications due to their long diffusion pathways, and the possibility of poor blockage leading to inaccessible regions of the material.

Finally, we note that these measurements have also been applied to the larger-pore Zn_2(dobpdc) framework.[15] Qualitatively similar spectra were obtained, though the increase in pore size from 15 to 22 Å led to an increase in $D_{//}$ by a factor of 4 to 6 across a range of CO_2 dosing pressures. These measurements therefore highlighted a straightforward means to tune transport properties through modification of the framework structure. Measurements and analysis for the Zn_2(dobpdc) sample interestingly also supported non-zero diffusion between the MOF pores, which was tentatively attributed to defects in the MOF structure enabling additional transport pathways.

Discussion

The case studies above highlight the power of NMR spectroscopy in revealing the chemistry of carbon dioxide capture. A particular success of the approach has been in studying the adsorption mechanisms that operate and the speciation of CO_2 in the captured state. In some cases NMR studies have revealed new adsorption mechanisms in CO_2 capture materials that were not readily accessible with other techniques. Moreover, diffusion measurements have been used to probe CO_2 transport mechanisms in capture materials.

A key limitation of much of the work to date is that it has largely been carried out under pure CO_2 conditions. For real-world CO_2 separations a mixture of gases is always present, not limited to CO_2, N_2, O_2, H_2O, CH_4, NO_X and SO_X. A number of initial efforts have been carried out to study mixed

gas adsorption, including CO_2/H_2O mixtures,[23,29,65] as well as CO_2/CH_4 mixtures.[49,66] The role of H_2O should be studied in particular, since various studies have highlighted that H_2O can have a significant impact on adsorption thermodynamics.[65] We further note that few studies have investigated CO_2 capture materials in the presence of O_2, despite O_2 often playing an important role in the oxidative degradation of many carbon capture materials.[67,68] Studies of adsorbent degradation in general have also been lacking.

A further limitation is that most of the NMR work to date has been carried out under *ex-situ* rather than *in situ* conditions. Time consuming *ex-situ* experiments often lead to a limited number of experimental conditions being sampled, and may result in temperature and pressure dependent phenomena being missed. Further method development will help to make *in situ* techniques more accessible and practical. Importantly, *in situ* measurements are well-suited to gas mixtures,[49] and should also enable kinetic studies, which have been rare to date.[43] We also note that low field NMR methods are being developed for the study of adsorption phenomena. The lower cost of these approaches are particularly attractive, and may be well-suited for industrial applications.[69] An important remaining challenge is to differentiate closely related adsorption products. As discussed above, the ^{13}C isotropic chemical shifts generally provide poor differentiation of ammonium carbamate, carbamic acid and bicarbonate species. Approaches that utilise additional NMR parameters, such as ^{13}C chemical shift anisotropies,[25] as well as ^{17}O NMR[14,70] may help to resolve closely related adsorption products in the future. The availability of increasingly high magnetic field strengths may make ^{17}O measurements particularly attractive.[71]

Finally, signal enhancement methods based on dynamic nuclear polarisation (DNP) may enable complex NMR measurements to be carried out without the need for isotopic enrichment. The use of exogenous radicals as polarising agents may perturb the CO_2 capture modes in some cases, though advances in the use of endogeneous radicals for DNP may be well suited for studies of CO_2 capture.[72] DNP methods may also allow for the enhancement of signals from species adsorbed at adsorbent particle surfaces, which may impact surface transport barriers.

Ultimately, further NMR method development may lead to breakthroughs in our understanding of CO_2 capture mechanisms, and could enable the design improved carbon capture materials that can help tackle the climate crisis.

Acknowledgements

References

1   M. Bui, C. S. Adjiman, A. Bardow, E. J. Anthony, A. Boston, S. Brown, P. S. Fennell, S. Fuss, A. Galindo, L. A. Hackett, J. P. Hallett, H. J. Herzog, G. Jackson, J. Kemper, S. Krevor, G. C. Maitland, M. Matuszewski, I. S. Metcalfe, C. Petit, G. Puxty, J. Reimer, D. M. Reiner, E. S. Rubin, S. A. Scott, N. Shah, B. Smit, J. P. M. Trusler, P. Webley, J. Wilcox and N. Mac Dowell, *Energy Environ. Sci.*, 2018, **11**, 1062–1176.

2   H.-O. Pörtner, D. C. Roberts, M. Tignor, E. S. Poloczanska, K. Mitenbeck, A. Alegría, M. Craig, S. Langsdorf, S. Löschke, V. Möller, A. Okem and Rama. B, *IPCC, 2022: Climate Change 2022: Impacts, Adaptation, and Vulnerability. Contribution of Working Group II to the Sixth Assessment Report of the Intergovernmental Panel on Climate Change*, Cambridge University Press. In Press.

3   B. Dutcher, M. Fan and A. G. Russell, *ACS Appl. Mater. Interfaces*, 2015, **7**, 2137–2148.

4   A. C. Forse and P. J. Milner, *Chem. Sci.*, 2021, **12**, 508–516.

5   E. S. Sanz-Pérez, C. R. Murdock, S. A. Didas and C. W. Jones, *Chem. Rev.*, 2016, **116**, 11840–11876.

6   S. Y. Lee and S. J. Park, *J. Ind. Eng. Chem.*, 2015, **23**, 1–11.

7   W. L. Theo, J. S. Lim, H. Hashim, A. A. Mustaffa and W. S. Ho, *Appl. Energy*, 2016, **183**, 1633–1663.

8   K. Sumida, D. L. Rogow, J. A. Mason, T. M. McDonald, E. D. Bloch, Z. R. Herm, T. H. Bae and J. R. Long, *Chem. Rev.*, 2012, **112**, 724–781.

9   D. M. D'Alessandro, B. Smit and J. R. Long, *Angew. Chemie - Int. Ed.*, 2010, **49**, 6058–6082.

10   J. Bin Lin, T. T. T. Nguyen, R. Vaidhyanathan, J. Burner, J. M. Taylor, H. Durekova, F. Akhtar, R. K. Mah, O. Ghaffari-Nik, S. Marx, N. Fylstra, S. S. Iremonger, K. W. Dawson, P. Sarkar, P. Hovington, A. Rajendran, T. K. Woo and G. K. H. Shimizu, *Science (80-.).*, 2021, **374**, 1464–1469.

11   E. J. Kim, R. L. Siegelman, H. Z. H. Jiang, A. C. Forse, J. H. Lee, J. D. Martell, P. J. Milner, J. M. Falkowski, J. B. Neaton, J. A. Reimer, S. C. Weston and J. R. Long, *Science (80-.).*, 2020, **369**, 392–396.

12   T. M. McDonald, J. A. Mason, X. Kong, E. D. Bloch, D. Gygi, A. Dani, V. Crocellà, F. Giordanino, S. O. Odoh, W. S. Drisdell, B. Vlaisavljevich, A. L. Dzubak, R. Poloni, S. K. Schnell, N. Planas, K. Lee, T. Pascal, L. F. Wan, D. Prendergast, J. B. Neaton, B. Smit, J. B. Kortright, L. Gagliardi, S. Bordiga, J. A. Reimer and J. R. Long, *Nature*, 2015, **519**, 303–308.

13   A. C. Forse, P. J. Milner, J. H. Lee, H. N. Redfearn, J. Oktawiec, R. L. Siegelman, J. D. Martell, B. Dinakar, L. B. Porter-Zasada, M. I. Gonzalez, J. B. Neaton, J. R. Long and J. A. Reimer, *J. Am. Chem. Soc.*, 2018, **140**, 18016–18031.

14   A. H. Berge, S. M. Pugh, M. I. M. Short, Z. Lu, J. Lee, C. J. Pickard and A. C. Forse, DOI:10.26434/chemrxiv-2021-09vcw-v2. 2022

15   A. C. Forse, M. I. Gonzalez, R. L. Siegelman, V. J. Witherspoon, S. Jawahery, R. Mercado, P. J. Milner, J. D. Martell, B. Smit, B. Blümich, J. R. Long and J. A. Reimer, *J. Am. Chem. Soc.*, 2018, **140**, 1663–1673.

16   W. Wang, W. D. Waang, B. E. G. Lucier, V. V. Terskikh and Y. Huang, *J. Phys. Chem. Lett.*, 2014, **5**, 3360–3365.

17   R. W. Flaig, T. M. Osborn Popp, A. M. Fracaroli, E. A. Kapustin, M. J. Kalmutzki, R. M. Altamimi, F. Fathieh, J. A. Reimer and O. M. Yaghi, *J. Am. Chem. Soc.*, 2017, **139**, 12125–12128.

18   R. Afonso, M. Sardo, L. Mafra and J. R. B. Gomes, *Environ. Sci. Technol.*, 2019, **53**, 2758–2767.

19   D. Shimon, C. H. Chen, J. J. Lee, S. A. Didas, C. Sievers, C. W. Jones and S. E. Hayes, *Environ. Sci. Technol.*, 2018, **52**, 1488–1495.

20   M. L. Pinto, L. Mafra, J. M. Guil, J. Pires and J. Rocha, *Chem. Mater.*, 2011, **23**, 1387–1395.

21   L. Mafra, T. Čendak, S. Schneider, P. V. Wiper, J. Pires, J. R. B. Gomes and M. L. Pinto, *J. Am. Chem. Soc.*, 2017, **139**, 389–408.

22   A. Sayari, A. Heydari-Gorji and Y. Yang, *J. Am. Chem. Soc.*, 2012, **134**, 13834–13842.

23   C. H. Chen, D. Shimon, J. J. Lee, F. Mentink-Vigier, I. Hung, C. Sievers, C. W. Jones and S. E. Hayes, *J. Am. Chem. Soc.*, 2018, **140**, 8648–8651.

24   R. Vieira, I. Marin-Montesinos, J. Pereira, R. Fonseca, M. Ilkaeva, M. Sardo and L. Mafra, *J.*

Phys. Chem. C, 2021, **125**, 14797–14806.

25   T. Čendak, L. Sequeira, M. Sardo, A. Valente, M. L. Pinto and L. Mafra, *Chem. - A Eur. J.*, 2018, **24**, 10136–10145.

26   C. H. Chen, E. L. Sesti, J. J. Lee, F. Mentink-Vigier, C. Sievers, C. W. Jones and S. E. Hayes, *J. Phys. Chem. C*, 2021, **125**, 16759–16765.

27   X. Kong, E. Scott, W. Ding, J. A. Mason, J. R. Long and J. A. Reimer, *J. Am. Chem. Soc.*, 2012, **134**, 14341–14344.

28   R. M. Marti, J. D. Howe, C. R. Morelock, M. S. Conradi, K. S. Walton, D. S. Sholl and S. E. Hayes, *J. Phys. Chem. C*, 2017, **121**, 25778–25787.

29   P. G. Boyd, A. Chidambaram, E. García-Díez, C. P. Ireland, T. D. Daff, R. Bounds, A. Gładysiak, P. Schouwink, S. M. Moosavi, M. M. Maroto-Valer, J. A. Reimer, J. A. R. Navarro, T. K. Woo, S. Garcia, K. C. Stylianou and B. Smit, *Nature*, 2019, **576**, 253–256.

30   Y. T. A. Wong, V. Martins, B. E. G. Lucier and Y. Huang, *Chem. - A Eur. J.*, 2019, **25**, 1848–1853.

31   J. J. Gassensmith, H. Furukawa, R. A. Smaldone, R. S. Forgan, Y. Y. Botros, O. M. Yaghi and J. F. Stoddart, *J. Am. Chem. Soc.*, 2011, **133**, 15312–15315.

32   M. E. Zick, S. M. Pugh, J.-H. Lee, A. C. Forse and P. Milner, *Angew. Chemie Int. Ed.*, , DOI:10.1002/anie.202206718.

33   P. J. Milner, R. L. Siegelman, A. C. Forse, M. I. Gonzalez, T. Runčevski, J. D. Martell, J. A. Reimer and J. R. Long, *J. Am. Chem. Soc.*, 2017, **139**, 13541–13553.

34   J. D. Martell, P. J. Milner, R. L. Siegelman and J. R. Long, *Chem. Sci.*, 2020, **11**, 6457–6471.

35   R. L. Siegelman, T. M. McDonald, M. I. Gonzalez, J. D. Martell, P. J. Milner, J. A. Mason, A. H. Berger, A. S. Bhown and J. R. Long, *J. Am. Chem. Soc.*, 2017, **139**, 10526–10538.

36   J. Xu, Y. M. Liu, A. S. Lipton, J. Ye, G. L. Hoatson, P. J. Milner, T. M. McDonald, R. L. Siegelman, A. C. Forse, B. Smit, J. R. Long and J. A. Reimer, *J. Phys. Chem. Lett.*, 2019, **10**, 7044–7049.

37   P. Rzepka, Z. Bacsik, A. J. Pell, N. Hedin and A. Jaworski, *J. Phys. Chem. C*, 2019, **123**, 21497–21503.

38   H. Thakkar, S. Eastman, A. Hajari, A. A. Rownaghi, J. C. Knox and F. Rezaei, *ACS Appl. Mater. Interfaces*, 2016, **8**, 27753–27761.

39   S. Chatterjee, S. Jeevanandham, M. Mukherjee, D. V. N. Vo and V. Mishra, *J. Environ. Chem. Eng.*, 2021, **9**, 105957.

40   T. H. Nguyen, S. Kim, M. Yoon and T. H. Bae, *ChemSusChem*, 2016, **9**, 455–461.

41   H. Yang, M. Singh and J. Schaefer, *Chem. Commun.*, 2018, **54**, 4915–4918.

42   H. Mao, J. Tang, J. Xu, Y. Peng, J. Chen, B. Wu, Y. Jiang, K. Hou, S. Chen, J. Wang, H. R. Lee, D. M. Halat, B. Zhang, W. Chen, A. Z. Plantz, Z. Lu, Y. Cui and J. A. Reimer, *Matter*, 2020, **3**, 2093–2107.

43   M. Wenzel, M. A. Zaheer, D. Issayeva, D. Poppitz, J. Matysik, R. Gläser and M. Dvoyashkin, *J. Phys. Chem. C*, 2021, **125**, 10219–10225.

44   M. Hunger, *Prog. Nucl. Magn. Reson. Spectrosc.*, 2008, **53**, 105–127.

45   J. Z. Hu, J. A. Sears, H. S. Mehta, J. J. Ford, J. H. Kwak, K. Zhu, Y. Wang, J. Liu, D. W. Hoyt and C. H. F. Peden, *Phys. Chem. Chem. Phys.*, 2012, **14**, 2137–2143.

46   B. Dinakar, A. C. Forse, H. Z. H. Jiang, Z. Zhu, J. H. Lee, E. J. Kim, S. T. Parker, C. J. Pollak, R. L. Siegelman, P. J. Milner, J. A. Reimer and J. R. Long, *J. Am. Chem. Soc.*, 2021, **143**, 15258–15270.

47   M. Aghaie, N. Rezaei and S. Zendehboudi, *Renew. Sustain. Energy Rev.*, 2018, **96**, 502–525.

48   M. Ramdin, T. W. De Loos and T. J. H. Vlugt, *Ind. Eng. Chem. Res.*, 2012, **51**, 8149–8177.

49   M. Sin, N. Kavoosi, M. Rauche, J. Pallmann, S. Paasch, I. Senkovska, S. Kaskel and E. Brunner, *Langmuir*, 2019, **35**, 3162–3170.

50   P. V. Kortunov, M. Siskin, L. S. Baugh and D. C. Calabro, *Energy and Fuels*, 2015, **29**, 5919–5939.

51   T. M. McDonald, W. R. Lee, J. A. Mason, B. M. Wiers, C. S. Hong and J. R. Long, *J. Am. Chem. Soc.*, 2012, **134**, 7056–7065.

52   H. Jo, W. R. Lee, N. W. Kim, H. Jung, K. S. Lim, J. E. Kim, D. W. Kang, H. Lee, V. Hiremath, J. G. Seo, H. Jin, D. Moon, S. S. Han and C. S. Hong, *ChemSusChem*, 2017, **10**, 541–550.

53   L. Frydman and J. S. Harwood, *J. Am. Chem. Soc.*, 1995, **117**, 5367–5368.

54   A. Medek, L. Marinelli and L. Frydman, *ACS Symp. Ser.*, 1999, **717**, 136–155.

55   R. E. Wasylishen, S. E. Ashbrook and S. Wimperis, Eds., *NMR of Quadrupolar Nuclei in Solid Materials*, John Wiley & Sons, Ltd., Chichester, 2012.

56   S. E. Ashbrook and S. Wimperis, *J. Magn. Reson.*, 2002, **156**, 269–281.

57   Z. Gan, *J. Am. Chem. Soc.*, 2000, **122**, 3242–3243.

58   M. Peksa, J. Lang and F. Stallmach, *Microporous Mesoporous Mater.*, 2015, **205**, 11–15.

59   M. Peksa, S. Burrekaew, R. Schmid, J. Lang and F. Stallmach, *Microporous Mesoporous Mater.*, 2015, **216**, 75–81.

60   A. C. Forse, K. A. Colwell, M. I. Gonzalez, S. Benders, R. M. Torres-Gavosto, B. Blümich, J. A. Reimer and J. R. Long, *Chem. Mater.*, 2020, **32**, 3570–3576.

61   C. R. Bowers, H. W. Long, T. Pietrass, H. C. Gaede and A. Pines, *Chem. Phys. Lett.*, 1993, **205**, 168–170.

62   L. C. Lin, J. Kim, X. Kong, E. Scott, T. M. McDonald, J. R. Long, J. A. Reimer and B. Smit, *Angew. Chemie - Int. Ed.*, 2013, **52**, 4410–4413.

63   P. T. Callaghan, *Principles of Nuclear Magnetic Resonance Microscopy*, Claredon Press, Oxford, 1992.

64   A. C. Forse, S. A. Altobelli, S. Benders, M. S. Conradi and J. A. Reimer, *J. Phys. Chem. C*, 2018, **122**, 15344–15351.

65   R. L. Siegelman, P. J. Milner, A. C. Forse, J. H. Lee, K. A. Colwell, J. B. Neaton, J. A. Reimer, S. C. Weston and J. R. Long, *J. Am. Chem. Soc.*, 2019, **141**, 13171–13186.

66   K. Roztocki, M. Rauche, V. Bon, S. Kaskel, E. Brunner and D. Matoga, *ACS Appl. Mater. Interfaces*, 2021, **13**, 28503–28513.

67   H. Liu, O. A. Namjoshi and G. T. Rochelle, *Energy Procedia*, 2014, **63**, 1546–1557.

68   C. S. Srikanth and S. S. C. Chuang, *ChemSusChem*, 2012, **5**, 1435–1442.

69   J. Marreiros, R. De Oliveira-Silva, P. Iacomi, P. L. Llewellyn, R. Ameloot and D. Sakellariou, *J. Am. Chem. Soc.*, 2021, **143**, 8249–8254.

70   J. H. Du, L. Chen, B. Zhang, K. Chen, M. Wang, Y. Wang, I. Hung, Z. Gan, X. P. Wu, X. Q. Gong and L. Peng, *Nat. Commun.*, 2022, **13**, 2–7.

71   E. G. Keeler, V. K. Michaelis, M. T. Colvin, I. Hung, P. L. Gor'Kov, T. A. Cross, Z. Gan and R. G. Griffin, *J. Am. Chem. Soc.*, 2017, **139**, 17953–17963.

72   A. Harchol, G. Reuveni, V. Ri, B. Thomas, R. Carmieli, R. H. Herber, C. Kim and M. Leskes, *J. Phys. Chem. C*, 2020, **124**, 7082–7090.